AGU PUBLICATIONS

Geochemistry, Geophysics, Geosystems

RESEARCH ARTICLE
10.1002/2013GC005165

Key Points:
- We investigate magnetomineral neoformation during Coe paleointensity experiments
- Linear Arai plots that pass pTRM checks are possible when neoformation occurs
- Such Arai plots yield underestimates of the true paleointensity

Supporting Information:
- Auxiliary Material
- ReadMe

Correspondence to:
Q. Liu,
qsliu@mail.iggcas.ac.cn

Citation:
Zhao, X., Q. Liu, G. A. Paterson, H. Qin, S. Cai, Y. Yu, and R. Zhu (2014), The effects of secondary mineral formation on Coe-type paleointensity determinations: Theory and simulation, *Geochem. Geophys. Geosyst.*, *15*, 1215–1234, doi:10.1002/2013GC005165.

Received 21 NOV 2013
Accepted 28 FEB 2014
Accepted article online 6 MAR 2014
Published online 23 APR 2014

The effects of secondary mineral formation on Coe-type paleointensity determinations: Theory and simulation

Xiangyu Zhao[1,2], Qingsong Liu[1], Greig A. Paterson[3], Huafeng Qin[1], Shuhui Cai[1], Yongjae Yu[4], and Rixiang Zhu[1]

[1]State Key Laboratory of Lithospheric Evolution, Institute of Geology and Geophysics, Chinese Academy of Sciences, Beijing, China, [2]Department of Earth and Environmental Sciences, Ludwig-Maximilians University, Munich, Germany, [3]Key Laboratory of Earth's Deep Interior, Institute of Geology and Geophysics, Chinese Academy of Sciences, Beijing, China, [4]Department of Geology and Earth Environmental Sciences, Chungnam National University, Daejeon, South Korea

Abstract Thellier-type experiments are the most widely applied approaches for determining the absolute paleointensities of Earth's magnetic field. One major problem, however, is that specimens are prone to thermal alteration due to the intensive thermal treatment during experiments. Linear Arai plots with acceptable partial thermal remanent magnetization (pTRM) checks have been considered as evidence for the absence of or negligible effects of thermal alteration and as reliable indicators of high-quality paleointensity estimates. However, by simulating the Coe variant of the Thellier method on assemblages of single domain (SD) magnetite particles, it is demonstrated that new magnetic minerals, which form during thermal treatments, can result in linear, concave-up, or concave-down Arai plots depending on the magnetic properties of both the primary and secondary magnetic phases. Among this range of behavior, pseudoideal Arai plots, which are linear with acceptable pTRM check statistics, would lead to paleointensity underestimates. It is further demonstrated that pTRM checks are proportional to the degree of underestimate with a magnetic granulometry dependency for SD particles. Due to the complexity of this dependency, pTRM check statistics are only comparable when specimens have similar magnetic properties. This suggests that a universal threshold for pTRM check statistics is not likely to be effective. Since the criteria of linearity and low pTRM check statistics are insufficient to guarantee the fidelity of the estimates auxiliary rock magnetic methods such as temperature-dependent hysteresis parameters and anhysteretic remanent magnetization are highly recommended to identify the presence of alteration.

1. Introduction

Absolute paleointensity data of Earth's magnetic field play an increasingly important role in exploring the evolution of Earth's interior [e.g., *Smirnov et al*., 2003; *Tarduno et al*., 2010]. Obtaining reliable paleointensity data is difficult because the experiments are time consuming and typically have a low success rate. The failure of paleointensity experiments can be caused by nonuniform magnetization in large magnetic grains [e.g., *Levi*, 1977], thermal alteration induced by heating during the laboratory experiment [e.g., *Coe*, 1967; *Kosterov and Prévot*, 1998], contamination of the natural remanent magnetization (NRM) by viscous or chemical remanent magnetizations [e.g., *Draeger et al*., 2006], or magnetic interactions between grains [e.g., *Wehland et al*., 2005].

Thellier-type double heating experiments are the most commonly used paleointensity methods [*Koenigsberger*, 1936; *Thellier and Thellier*, 1959; *Coe*, 1967; *Aitken et al*., 1988; *Tauxe and Staudigel*, 2004; *Yu et al*., 2004]. These methods rely on Néel's theory of thermal remanent magnetization (TRM) for single domain (SD) grains [*Néel*, 1949], which states that the TRM acquired by an assemblage of noninteracting SD magnetic particles is, to first approximation, linearly proportional to the weak applied fields (i.e., field strengths on the order of Earth's magnetic field). *Thellier and Thellier* [1959] designed a stepwise heating procedure based on the fact that the magnetic assemblages within natural specimens often have a wide range of unblocking temperatures (T_{ub}) above which SD particles become superparamagnetic and lose their remanence. In a Thellier-Thellier experiment, the NRM of a specimen is progressively replaced by a laboratory partial TRM (pTRM) that is imparted in a known field (B_{lab}). Linearity of TRM acquisition with the applied field allows the strength of the ancient field (B_{anc}) to be estimated by:

$$\frac{B_{lab}}{B_{anc}} = \frac{TRM}{NRM}$$

It is common practice to plot the data on an Arai plot [*Nagata et al*., 1963] where NRM remaining and pTRM gained after each step are compared. For a hypothetical ideal paleointensity specimen, which consists of thermally stable noninteracting SD particles, a best fit linear line can be fitted to any portion of the Arai plot and will yield a slope equivalent to the ratio of B_{anc} to B_{lab}. When the bulk magnetic properties of a specimen change, such as may occur if the magnetic mineralogy chemically alters during laboratory heating, the linearity of the Arai plot may not be preserved [e.g., *Tauxe and Love*, 2003]. Several studies, however, have demonstrated that alteration can sometime only affect part of an Arai plot and that a portion can remain linear even in the presence of laboratory alteration [e.g., *Prévot et al*., 1983; *Kono*, 1987]. To detect such a situation, the pTRM check, a repeat remagnetization step, has been adopted as a standard test to monitor alteration in all thermal paleointensity experiments [*Prévot et al*., 1983]. The pTRM check is designed to identify changes in the ability of a specimen to acquire pTRM in blocking temperature (T_b) ranges below the temperature of the check and was first proposed by *Thellier and Thellier* [1959], who involved a repeat check to the same temperature as the experiment progressed. In its modern form [*Prévot et al*., 1985], the pTRM check is performed in "sliding-window" fashion whereby the temperature at which the check is performed increases as the experiment progresses. In the framework of a Coe protocol experiment [*Coe*, 1967], the first in-field heating step in the original Thellier-Thellier method is replaced by a zero-field demagnetization step, which allows the NRM remaining to be directly measured rather than calculated via vector arithmetic. The basic operational sequence at each step (T_j) is as follows: first, the total magnetization (the sum of remaining NRM and any previously imparted TRM) with $T_{ub} < T_j$ is erased by heating and cooling a specimen between room temperature (T_0) and T_j in zero-field, after which the remaining NRM is measured at T_0. Second, $pTRM(T_0,T_j)$ is acquired by reheating the specimen to T_j and cooling it to T_0 in field. When a pTRM check is required, a pTRM is imparted to a lower temperature, say T_i, after the NRM demagnetization to T_j, but before $pTRM(T_0,T_j)$ is acquired. Such a check is referred to as $pTRM'_j(T_0,T_i)$ hereafter.

The scalar difference between $pTRM'_j(T_0,T_i)$ and $pTRM(T_0,T_i)$ is used in a broad range of statistics to quantify the reliability of the data obtained [see the Standard Paleointensity Definitions (SPD) for a complete listing; *Paterson et al*., 2014]. Generally speaking, a smaller pTRM check difference is considered as indicative of higher quality data. Typical critical thresholds used for data selection, however, are defined in a somewhat arbitrarily fashion and lack a solid theoretical basis. From a practical point of view, the thresholds should not be too strict otherwise ideal specimens, which are subject to ever present experimental noise, will be rejected [e.g., *Paterson et al*., 2012; *Paterson*, 2013]. On the other hand, significant errors in paleointensity estimates could be introduced if the critical thresholds are too tolerant. Refining our understanding of how magnetomineralogical alteration manifests in paleointensity data is an important step to asserting the fidelity of the data obtained.

In this study, we present a new model based on Néel theory [*Néel*, 1949] to investigate the formation of new magnetic phases during the heating required in a Coe paleointensity experiment. We use the model to investigate how newly formed magnetic particles change the pTRM spectrum of a specimen and thus affect the Arai plot behavior. We also quantify the degree of secondary magnetic phase formation that is required to maintain linear Arai plots and relate the resultant paleointensity estimates to the corresponding pTRM checks to assess the reliability of these checks.

2. Paleointensity Theory for a Coe Protocol Simulation

2.1. Néel Theory

From Néel's theory of magnetism [*Néel*, 1949], the magnetic relaxation time (τ) for noninteracting uniaxial SD magnetic grains is given by:

$$\tau = \tau_0 \exp\left(\frac{E_b}{k_B T}\right), \quad (1)$$

where τ_0 is the characteristic time of thermal fluctuations ($\tau_0 \approx 10^{-9}$ s), k_B is the Boltzmann constant

($k_B = 1.38 \times 10^{-23}$ J/K), T is the temperature, and E_b is the energy barrier inhibiting changes in the magnetization. The energy barrier to coherent rotation of magnetizations in SD grains is given by:

$$E_b(T) = \frac{1}{2} V M_s(T) B_k(T) \left(1 - \frac{|\vec{B}_0|}{B_k(T)}\right)^2, \tag{2}$$

where M_s is the saturation magnetization, B_k ($= \mu_0 H_k$) is the microscopic coercivity, V is the grain volume, and $\vec{B}_0$ is the applied field. Using the weak field approximation, when $|\vec{B}_0| \ll B_k$, equation (2) can be simplified to:

$$E_b(T) = \frac{1}{2} V M_s(T) B_k(T). \tag{3}$$

The energy barrier of a particle prevents its magnetization from disordering over time scales less than the relaxation time. As the temperature decreases, a magnetic particle will experience less thermal agitation, and the height of the energy barrier will increase due to increased M_s and B_k. The net effect is that relaxation time will become longer and at a critical temperature, known as the blocking temperature, the relaxation time will become much longer than the typical laboratory measurement time scale (τ_m) and the magnetization of the grain will become locked in. For a given time scale of τ_m, the blocking temperature (T_b) of a particle with $M_s(T_0)$ and $B_k(T_0)$ is:

$$\frac{T_b}{\beta^2(T)} = \frac{V M_s(T_0) B_k(T_0)}{2 k_B \ln\left(\frac{\tau_m}{\tau_0}\right)} \left(1 - \frac{|\vec{B}_0|}{B_k(T_0)\beta(T_b)}\right)^2, \tag{4}$$

where T_0 is room temperature and $\beta(T) \equiv M_s(T)/M_s(T_0)$ [*Dunlop and Özdemir*, 1997]. From this T_b can be numerically solved.

TRM is acquired by a magnetic grain when it cools down through its T_b in the presence of a magnetic field. For an assemblage of randomly oriented identical SD grains with dominant uniaxial anisotropy, the TRM at temperature T ($< T_b$) can be expressed by:

$$M_{tr}(T) = M_{rs}(T) \tanh\left(\frac{M_s(T_b) V |\vec{B}_0|}{k_B T_b}\right), \tag{5}$$

where $M_{rs}(T)$ is the saturation remanent magnetization at T [*Dunlop and Özdemir*, 1997]. Conversely, a particle can be demagnetized as it is heated in zero-field above its T_{ub} for a period of time longer than its relaxation time. In the strictest sense, since unblocking occurs in zero-field, but blocking occurs in an applied field, $T_{ub} \neq T_b$. This temperature difference, however, is small (typically $<2^\circ$C) and for paleointensity experiments, has a negligible effect [*McClelland and Briden*, 1996; *Dunlop and Özdemir*, 1997; *Paterson et al.*, 2012].

2.2. Simulation of Coe-Type Protocol Experiments

In natural specimens, magnetic particles consist of grains with various volumes and coercivities. Let $f(T)$, $g(V)$, and $h(B_k)$ represent the distributions of blocking temperature, grain size, and coercivity, respectively. These distributions can be related as follows:

$$\int_{T<T_C} f(T)dT = \int_V \int_{B_k} g(V)h(B_k)dV dB_k = 1. \tag{6}$$

Microscopic coercivity, however, also depends on the shape of particles. Elongated magnetite particles have much larger B_k than spherical particles with the same volume. Even if the aspect ratios are identical, smaller particles have smaller effective coercivities due to thermal agitation [*Dunlop and Özdemir*, 1997].

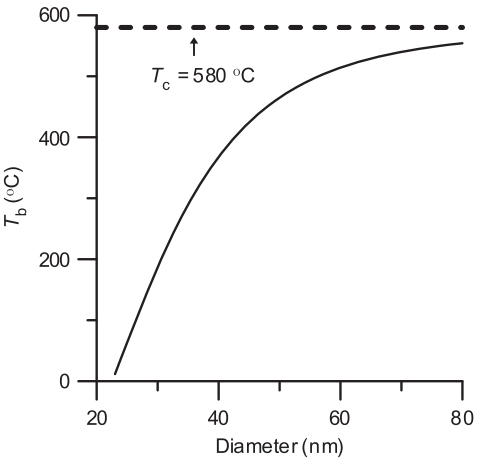

Figure 1. Relationship between blocking temperature and grain size for SD magnetite (B_k = 60 mT). The strength of ambient magnetic field is set to be 100 μT. The dashed line indicates the Curie temperature of magnetite.

Thus, $h(B_k)$ is also a function of $g(V)$. For simplicity, we model uniaxial grains with a constant B_k of 60 mT, which is equivalent to a length to width ratio of 1:1.3. In this case, equation (6) becomes:

$$\int_{T<T_C} f(T)dT = \int_V g(V)dV = 1. \tag{7}$$

With this approximation, T_b only depends on the volume of the particles (Figure 1) (i.e., $T_b = T_b(V)$), thus T_b can be converted to blocking volume (V_b), which is the SP/SD threshold at T_b. We note that a specimen's T_b spectrum is the main factor controlling its Arai plot behavior. T_b spectra, however, are nonunique and the same spectrum can be derived from differing combinations of distributed or fixed volumes or coercivities. By choosing a fixed B_k, we simplify the modeling process by having only one variable, volume. This simplification does not change the overall results of our simulations since the equivalent T_b spectra that we model can be derived from alternative volume or coercivity values.

The pTRM, $pTRM(T_0,T_i)$, is the sum of all partial TRMs carried by particles with $T_b < T_i$, or $V < V_b(T_i)$, where $V_b(T_i)$ is the blocking volume at T_i. NRM carried by SD particles with $V < V_b(T_i)$ can be demagnetized up to T_i, but is similarly remagnetized by in-field heating and cooling to T_i, which can be described by:

$$pTRM(T_0, T_i) = \int_{V_b(T_0)}^{V_b(T_i)} g(V) M_{tr}(T_0, V) V dV, \tag{8}$$

where $M_{tr}(T_0, V) = M_{rs}(T_0)\tanh\left(\frac{M_s(T_b)V|\vec{B}_0|}{k_B T_b}\right)$ and T_b itself is also a function of V.

This description of pTRM gained is also valid for pTRM acquisition during check steps. A pTRM check can then be defined as the scalar difference between the original pTRM and the check (pTRM′):

$$\delta pTRM_{i,j} = pTRM'_j(T_0, T_i) - pTRM(T_0, T_i), \tag{9}$$

This raw value, however, is not used to select data directly and is typically normalized by one of a range of other statistics. Some of the common methods of normalizing $\delta pTRM_{i,j}$ are introduced in section 4, but details are given in SPD [*Paterson et al.*, 2014].

For natural specimens, it is reasonable to assume that the magnetic particle volume distribution can be represented by a lognormal distribution [*Worm*, 1998]:

$$g(V; \mu, \sigma) = \frac{1}{\sqrt{2\pi}\sigma V}\exp\left(-\frac{(\ln V - \mu)^2}{2\sigma^2}\right), \tag{10}$$

where μ and σ are the location and scale parameters, respectively. These correspond to the mean and standard deviation of the underlying normal distribution. We use this type of grain size distribution (GSD) in the model.

2.3. Neoformation of Magnetic Particles

Newly formed magnetic phases are often considered responsible for increases in a specimen's pTRM capacity [e.g., *Prévot et al.*, 1983, 1985]. One possible source of neoformation is clay minerals that can form through the weathering igneous rocks [e.g., *Zhou et al.*, 2001]. Iron-bearing clay minerals are susceptible to

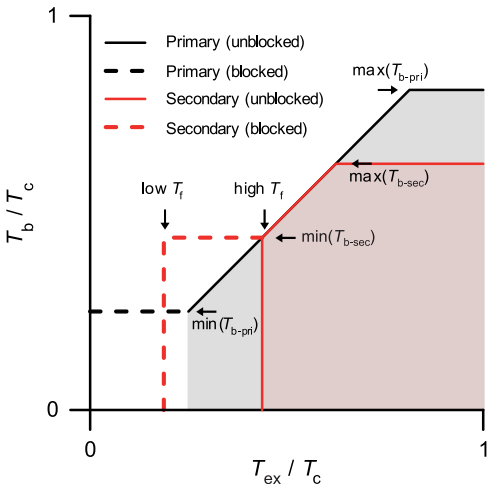

Figure 2. Schematic of the TRM acquisition of the alteration model. The horizontal axis indicates the peak temperature of the experiment (T_{ex}). The vertical axis represents the blocking temperature (T_b). Both are normalized by Curie temperature (T_c). SD particles stay blocked (horizontal dashed lines) when $T_{ex} < \min(T_b)$. As T_{ex} increases, particles are gradually activated (indicated by the solid diagonal line) and entirely unblock at $T_{ex} = \max(T_{b\_pri})$, thus T_b does not increase any more (solid horizontal lines). Black and red lines represent the primary and secondary components, respectively. The vertical dashed line indicates the formation temperature (T_{f_low}) of a secondary phase that is formed in the blocked state. The vertical solid line indicates the presence of an unblocking secondary phase at T_{f_high}. The illustrated secondary phases start to acquire pTRM when $T_{ex} \geq \min(T_{b\_sec})$ and the secondary pTRM reaches the maximum when $T_{ex} = \max(T_{b\_sec})$. The slope of the Arai plot is affected between $\min(T_{b\_sec})$ and $\max(T_{b\_sec})$. TRM contributions from the primary and secondary components are indicated by gray and red shaded areas, respectively. The red region is superimposed on the gray one.

thermal alteration that can produce magnetic phases that result in magnetic enhancement [e.g., *Zhang et al.*, 2012]. The models that we present here focus on these types of alteration mechanisms, whereby new magnetic minerals form without affecting the primary minerals.

Our simulations are restricted to the Coe paleointensity protocol [*Coe*, 1967]. To simplify the modeling, we focus on the first order effects of the neoformation on the paleointensity estimation and make the following assumptions to avoid possible situations that involve CRM and TCRM: (1) the primary magnetic minerals (PMMs) are not subject to chemical alteration since they have been relatively stabilized during geological time compared with the newly formed secondary magnetic minerals (SMMs); (2) the SMMs, if any, are only formed during first heating-cooling cycle, which is in zero-field so that particles are formed without acquiring a CRM or TCRM; (3) the SMMs are allowed to further alter only at temperatures higher than their formation temperature (T_f), and any further alteration is also restricted to the zero-field steps; (4) it is assumed that any pTRM carried by the SMMs is thermally demagnetized before additional growth and therefore no TCRM is acquired. Under these assumptions, the (un)blocking temperature spectra of the PMMs are independent of the neoformation of the SMMs. Therefore, the total TRM gained is the linear sum of the TRMs carried by the PMMs and SMMs.

The basic concept of the model is schematically demonstrated in Figure 2. PMMs, indicated in black, do not gain TRM while blocked (dashed line) until the experimental temperature (T_{ex}) exceeds the minimum T_b of the PMMs ($T_{b\_pri\_min}$). The NRM is then gradually replaced by TRM until all PMMs unblock at $T_{b\_pri\_max}$. This process is indicated by the black shaded area under the solid line. SMMs (indicated in red) produced at T_f on the other hand, are blocked (horizontal dashed line) until $T_{ex} > \max(T_f, T_{b\_sec})$. Notice that the condition of $T_f > T_{b\_sec}$ means that SMMs are formed in an unblocked state, thus are capable of acquiring remanence. As the experiment progresses to higher T_{ex}'s, the SMMs continue to acquire TRM, which reaches a maximum when $T_{ex} \geq T_{b\_sec\_max}$. This is indicated by the shaded area under the solid line.

For simplicity, we assume that the newly formed magnetic particles have the same B_k as that of the PMMs, whereby the T_b spectra of both PMMs and SMMs are entirely controlled by the GSDs (equation (7)). The progressive formation of new magnetite particles can therefore be simulated by progressively adjusting the GSD of the SMMs. If we further assume that the GSD of the SMMs formed at each step also follows the log-normal distribution ($g(V;\mu,\sigma)$), which can be represented by three parameters: concentration (c is the ratio of the number of new magnetic grains to the number of primary magnetic grains, i.e., $c = 1$ for the GSD of the PMMs), location (μ, which corresponds to a median volume of $\exp(\mu)$), and shape (σ, which control the width of the distribution; cf., equation (10)). For example, at the ith step of the paleointensity experiment, the GSD of the SMMs is described as $c_i g_i(V;\mu_i,\sigma_i)$. $c_i = 0$ when neoformation is absent.

There are numerous growth scenarios that the SMMs could undergo after formation. We focus on two representative possibilities termed as the static-accumulation model and the dynamic-growth model, respectively. The static-accumulation model states that particles formed at T_i remain stable through all subsequent steps. Therefore, SMMs that form at T_i are independent of those that form during other heating

steps. In this sense the GSD of the bulk specimen (PMMs + SMMs) can be described as a sum, whereby the effective GSD at T_i, $g^*(V,T_i)$, is described by:

$$g^*(V,T_i)=g_{\mathrm{pri}}\left(V;\mu_{\mathrm{pri}},\sigma_{\mathrm{pri}}\right)+\sum_{k=0}^{i}c_k\cdot g_k(V;\mu_k,\sigma_k),\qquad i=0,1,2,\ldots \tag{11}$$

where $g_{\mathrm{pri}}(V;\mu_{\mathrm{pri}},\sigma_{\mathrm{pri}})$ is the GSD of the PMMs and $c_0 = 0$ (i.e., there is no secondary mineral formation in the unheated specimen).

An alternative scenario is that the newly formed particles continue to grow in size or increase in absolute concentration at higher temperatures. In this case, the SMMs formed at different steps are not always independent. For simplicity, however, we maintain the assumption that at each step the GSD of the SMMs follows a log-normal distribution, that is, the secondary GSD at the *i*th step of the experiment, given by $c_i g_i(V;\mu_i,\sigma_i)$, is a single component instead of sum of previous GSDs and will then evolve to $c_{i+1}g_{i+1}(V;\mu_{i+1},\sigma_{i+1})$ at step $i + 1$. Therefore the effective GSD at T_i in the dynamic-growth model is:

$$g^*(V,T_i)=g_{\mathrm{pri}}\left(V;\mu_{\mathrm{pri}},\sigma_{\mathrm{pri}}\right)+c_i\cdot g_i(V;\mu_i,\sigma_i),\qquad i=0,1,2,\ldots \tag{12}$$

It should be noted that these two scenarios are related to each other. For instance, equations (11) and (12) become equivalent if μ and σ are fixed at all temperatures with varying c. In this sense, the static accumulation model can be viewed as a special case of the dynamic-growth model. In both cases, g^* is used to calculate pTRM, but only g_{pri} is used to determine the NRM.

2.4. The Experiment and Analysis

In our model, we simulate Coe protocol experiments with 16 temperature steps between T_0 and T_c (= 580°C). The steps are widely spaced (100, 200, and 300°C) below 350°C, the step interval decreases to 25°C for $350°C \leq T_{ex} \leq 475°C$ and 15°C for $T_{ex} > 475°C$. pTRM checks are carried out at every step. For Arai plot line-fitting, unless otherwise stated, all points on the Arai plot are used to obtain the paleointensity estimate.

Concerning the shape of the Arai plots, the Arai plot curvature can serve as a quantification of nonlinearity [*Paterson*, 2011]. The curvature ($\vec{k}$), obtained by a best fit circle to pairs of NRM-TRM data, is positive when the curve is concave-up and negative when concave-down. The quality of the fit can be assessed by the sum of squares of the errors (SSE). These parameters are used for assessment of the shape of Arai plots in the next section.

In addition to standard pTRM check statistics, the normalized room temperature M_{rs} of the bulk specimen after each heating [*Qin et al.*, 2011] is incorporated for monitoring alteration. Under the assumptions that magnetite is the only magnetic mineral and that the PMMs are stable during the entire experiment, this parameter is defined as:

$$M_{\mathrm{rs\_norm}}(T_0,T_i,V)=\frac{M_{\mathrm{rs}}(T_0)V_{\mathrm{SD}}(T_i)}{M_{\mathrm{rs}}(T_0)V_{\mathrm{SD}}(T_0)}=\frac{V_{\mathrm{SD}}(T_i)}{V_{\mathrm{SD}}(T_0)}=1+\frac{V_{\mathrm{SD\_SMM}}(T_i)}{V_{\mathrm{SD\_PMM}}}, \tag{13}$$

where $V_{\mathrm{SD}}(T_i)$ is the total volume of SD magnetite (determined at T_0) after heating to T_i, therefore $V_{\mathrm{SD}}(T_0)$ is the volume of PMMs ($V_{\mathrm{SD\_PMM}}$) and $V_{\mathrm{SD\_SMM}}$ denote the volumes of SD components of SMMs at T_0. This parameter is a function of the relative concentration of all SD SMMs after heating to T_i regardless of their T_b's and is therefore more sensitive to alteration than the pTRM check, which is only affected by magnetic minerals with $T_b \leq T_i$.

3. Simulation Results

The effects of T_f, the T_b distribution and concentration of the SMMs on the shape of the Arai plot are demonstrated in this section. We set $B_{\mathrm{anc}} = B_{\mathrm{lab}} = 100$ μT and the fields are oriented parallel to each other. We note that for all of our simulations, 100 μT is within the field range for approximately linear TRM acquisition.

For all simulations, we assume that $B_k = 60$ mT for both the PMMs and the SMMs, and that the GSD of the PMMs has a median grain size (D_{median}) of 45 nm with $\sigma_{pri} = 0.4$; the corresponding T_b ranges from ~300 to 520°C (Figure 3a, black). The GSDs of SMMs vary from case to case. The relationship between T_b and the particle diameter ($D = (6V/\pi)^{1/3}$) of SD magnetite is shown in Figure 1. The T_b spectrum is no longer log-normal due to the nonlinear transform.

3.1. The Static-Accumulation Model

The static-accumulation model consists of independent alteration steps that happen at each initial heating (i.e., only the first heating to a given temperature). To simply illustrate the effects of this style of alteration, examples of the elementary static case where neoformation takes place only once are presented.

In the first two cases, the SMMs with a narrow T_b distribution (Figure 3a, blue) are simulated. D_{median} of the SMMs is 45 nm (equivalent to $T_{b\_median} = 424$°C) and σ is 0.05. This distribution is so narrow that >99% of the SMMs unblock within $400°C < T < 450°C$. The concentration is set such that the total volume of the SMMs is 10% of the PMMs by volume. In these examples, we consider two different formation temperatures (T_f): $T_f = 100$ and 475°C (i.e., one below and the other above T_{b_median}). When the SMMs are formed at $T_f = 100$°C, the Arai plot is unaffected until T_{ex} reaches 425°C (Figure 3c, blue). Above T_{b_median}, unblocked SMMs increase the pTRMs gained at the 425 and 450°C steps and the Arai plot slope shallows. Above the 450°C step, however, the slope returns to the expected value of −1 because no additional pTRM is acquired by the SMMs (cf. Figure 2a, red solid horizontal line). It should be noted that the pTRM checks at all steps are identical to the original ones (i.e., the alteration is invisible to the pTRM check), while the change in M_{rs} at $T_{ex} = 100$°C is obvious (Figure 3b, circle). In contrast, when the SMMs are formed at $T_f = 475$°C, the Arai plot (Figure 3d, solid line) is unaffected up to the step before the SMMs form (450°C). Above 475°C, the Arai plot data match the $T_f = 100$°C case (Figure 3d, dashed line) because the volume of unblocked SMMs is identical. However, the neoformation is visible to the pTRM check at 450°C as well as M_{rs}. These cases illustrate three main points.

1. It is the SMMs with $T_b < T_i$ that distort the shape of Arai plots when they acquire pTRM.

2. The amount of distortion is modulated by the total volume of the unblocked SMMs.

3. It is the unblocked parts of SMMs that are visible to pTRM checks, in other words, pTRM check will fail to identify alteration if all SMMs are in a blocked state during checks. Changes in M_{rs}, however, will be observed.

For natural specimens, a wide T_b distribution should be expected, thus we replace σ in the previous cases with a larger value of 0.35 to demonstrate the effect of a wide distribution. D_{median} and the total volume of SMMs are kept unchanged so that the M_{rs}-T curve is identical for all cases. For $T_f = 100$°C, the alteration is still invisible to pTRM check, but the corresponding Arai plot (Figure 3e, red solid line) is more linear with $\vec{k} = -0.0152$ when compared to $\vec{k} = -0.0834$ for the narrow case (Figure 3e, blue dashed line). For $T_f = 475$°C, the Arai plot for the wide-T_b case has a larger $\vec{k}$ than the narrow case, but the difference between the pTRM check and the original pTRM at 450°C is smaller. This is because the proportion of unblocked SMMs below 450°C decreases as the T_b distribution broadens. These results suggest that a more progressive unblocking process may result in higher $\vec{k}$ and smaller pTRM check differences than for the extremely narrow T_b case.

In the next two examples, neoformation occurs at every T_{ex} from above 300°C and the general behavior of the static-accumulation model is illustrated (Figure 4). As T_{ex} increases, SMMs are introduced with $T_{b\_median} > T_{ex}$ and a moderate distribution width ($\sigma = 0.15$). By such a setup, the majority of SMMs are formed in a blocked state and the pTRM check statistics are negligible (e.g., Figure 4c). The T_{b_median}-T_{ex} relationship for the SMMs in both cases are identical, however, the concentrations vary with temperature in different patterns. In case 1 (Figure 4c, c1), more abundant SMMs form at lower T_{ex}'s than case 2 (Figure 4d, c2), therefore the final T_b distribution of c1 has more SMMs with low T_b as shown in Figure 4a (blue for c1 and red for c2). Curves of M_{rs} versus T_{ex} and their derivatives are shown in Figure 4b. The large production of SMMs occurs at the 425°C step in c1 and at the 475°C step in c2, the total volumes of the SMMs become equivalent (at 20% of the PMMs) from above 500°C. Due to the fact there are more SMMs with relatively low T_b, the Arai plot of c1 (Figure 4c) deviates from the expected trend at lower temperatures than for c2 (Figure 4d). Due to the appropriate combinations of concentrations, the Arai plot ends up visually linear. The paleointensity estimate for

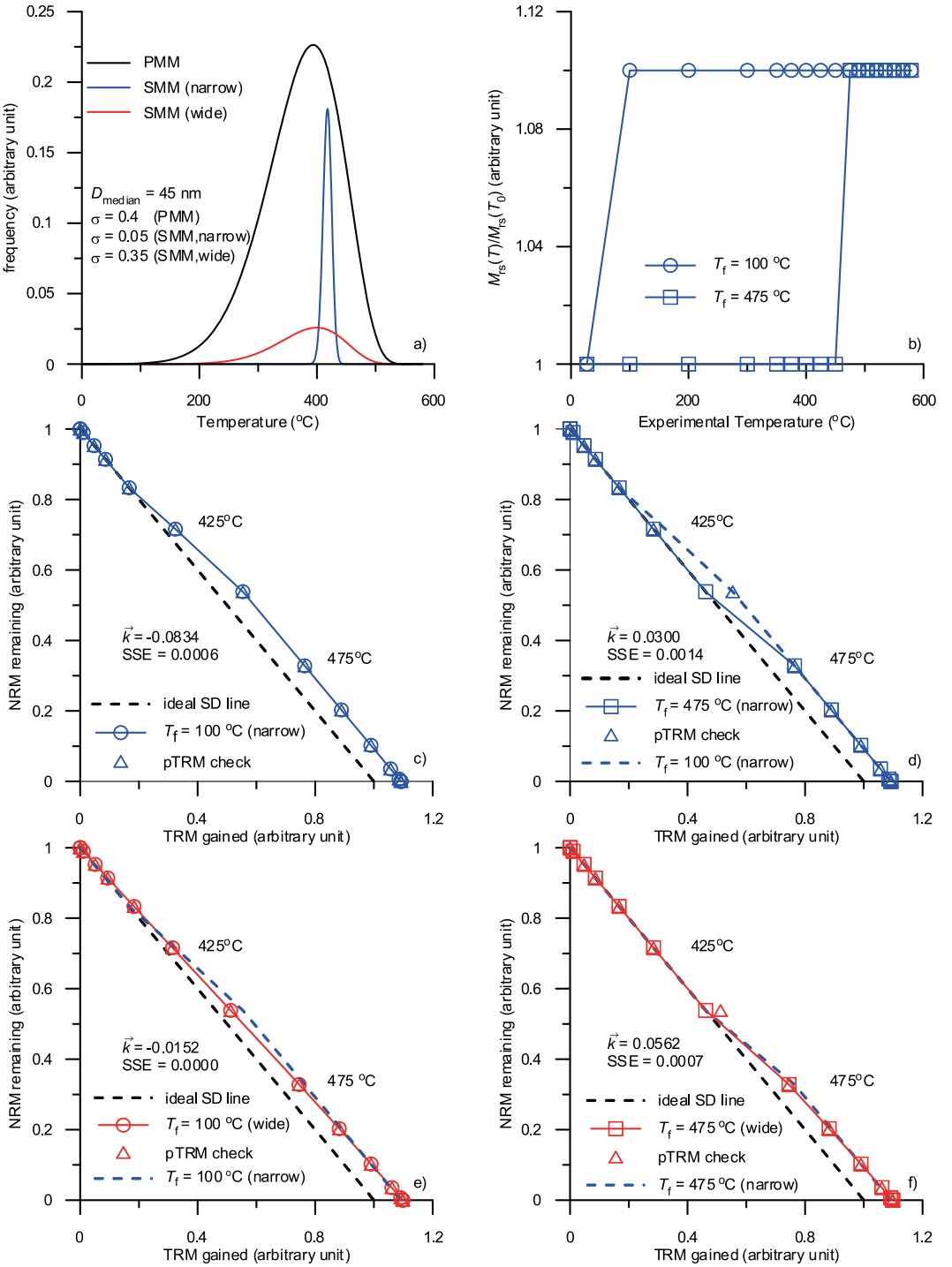

Figure 3. Four basic scenarios of the static-accumulation model. In each scenario, neoformation is allowed only once at one of the two possible formation temperatures (T_f = 100 or 475°C). (a) The median diameter of the secondary phase is fixed to 45 nm, but two shapes of distribution are considered, one is narrow (σ = 0.05) and the other is wide (σ = 0.35). (b) Despite the different shapes, the total volume, indicated by the maximum of normalized M_{rs}, of the secondary phase in each case is identical with each other. The curve with open circles is the variation of M_{rs} for cases with T_f = 100°C. The curve with squares is for cases with T_f = 475°C. They merge above 475°C. Arai plots for the narrow distribution cases with (c) low T_f and (d) high T_f, and the wide distribution cases ((e) for low T_f, (f) for high T_f). On each Arai plot, the dashed curves serve as references for comparison (i.e., the dashed curve in (d) is the blue curve in (c), which is the case with narrow GSD formed at 475°C).

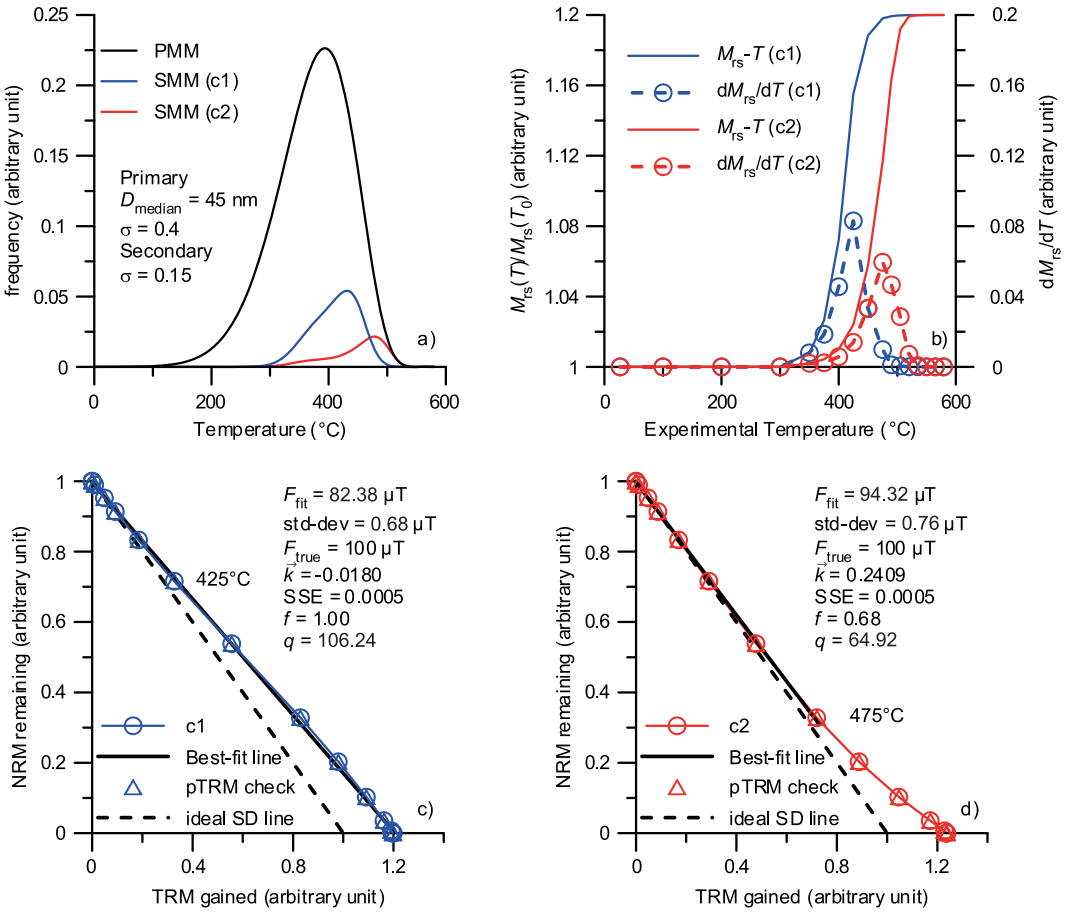

Figure 4. Effects of varying concentration of the SMMs on Arai plots. These results are from the static-accumulation model and $T_f < T_{b\_median}$ at almost every step. Neoformation occurs above 300°C with varying median diameters (D_{median}), but with the same $\sigma = 0.15$. The T_b distribution of the PMMs and final SMMs of both cases are shown in Figure 4a. D_{median}'s for SMMs at each step are identical in c1 and c2 and are set such that the respective T_{b_median} is higher than the T_f. Therefore, SMMs are produced in a blocked state. The only difference between the two cases is the concentration at each step, which is demonstrated in Figure 4b by M_{rs} versus T_{ex} (solid lines) and their derivatives (dashed lines with circles). There are more abundant SD SMMs produced in c1 below 500°C. Since $T_f < T_{b\_median}$, the pTRM checks fail to detect the neoformation.

case 1 is 82.38 μT. In case 2, since fewer SMMs unblock below 475°C, the section between T_0 and 475°C of c2 yields a closer estimate of 94.32 μT with respect to a true field of 100 μT. NRM fraction (f), the quality factor (q) are also listed in the figures [see SPD for details; *Paterson et al.*, 2014].

3.2. The Dynamic-Growth Model

In the static-accumulation models, the pTRM checks are never smaller than the original pTRMs. This is due to the fact the volume of the SMMs with $T_b < T_{ex}$ does not decrease. If, however, the grain size of the SMMs evolves with temperature (i.e., each individual grain grows), then the T_b distribution at the previous step will shift toward higher temperatures. In this section, we consider two specific examples to highlight how the evolution of the SMMs affects the shape of an Arai plot and the pTRMs checks. In both cases, the T_b distribution ($\sigma = 0.05$) of the SMMs between two adjacent steps are set such that the overlap is at a minimum (Figure 5a, dash-dot curves), which represents a fast grain growth scenario. The total volume of SMMs remains constant after they form at $T_f = 350$°C (Figure 5b), however, the growth rates are different between the two cases.

In the first example (d1), T_{b_median} of the SMMs is always lower than T_{ex} (Figure 5c). On the corresponding Arai plot (Figure 5d) a clear deviation from the expected slope can be seen immediately after neoformation happens at T_f. Above T_f, the slope remains constant because the volume of unblocked SMMs does not change. However, when pTRM checks are carried out to lower temperatures, they are smaller than the original pTRMs since the volume of SMMs with lower T_b has decreased as T_{b_median} increases.

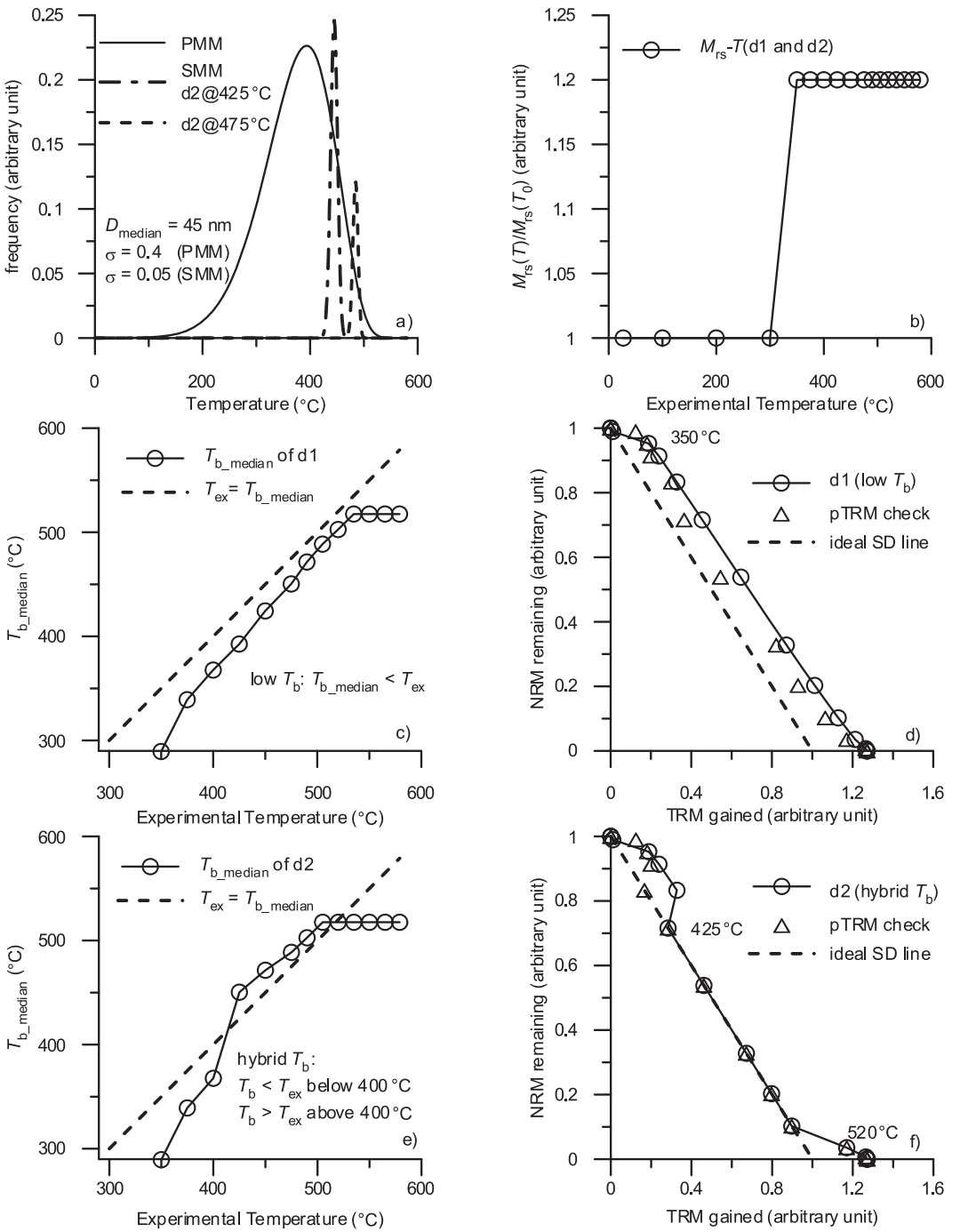

Figure 5. Two basic scenarios for the dynamic-growth model. In each case, neoformation first occurs at 350°C. In the following steps, the grain size of the SMMs increases as the temperature increases. (a) The T_b distributions of the SMMs of d2 at 425 and 475°C are shown together with that of the PMMs. In both cases, though grain size is growing, the total volume of the SD SMMs are kept constant above 350°C, as shown by the variation of M_{rs} in Figure 5b. The volume of SMMs is 20% of the PMMs. (c) The median T_b of SMMs versus the experimental temperature (T_{ex}) for d1. The curve lies below the diagonal, which means SMMs are in an unblocked state at each step (i.e., $T_{b\_median} < T_{ex}$). The corresponding Arai plot (d) deviates from the ideal SD line above 300°C where the neoformation starts. The pTRM checks are smaller than the original pTRMs above 350°C due to the fact that parts of SMMs with lower T_{b_median} are vanishing as T_{ex} increases. In contrast, in the case of d2 where the $T_{b\_median} > T_{ex}$ between 425 and 505°C (shown in Figure 5e), the corresponding segment on the Arai plot (f) coincides with the ideal SD line despite deviations at the low and high temperature ends where the SMMs are in unblocked state.

In the second example (d2), T_{b_median} of SMMs are identical to d1 until the 425°C step, where T_{b_median} increases sharply so that the SMMs shift from the unblocked state to the blocked state (Figure 5e). The abrupt change in growth rate results in a hump on the Arai plot (Figure 5f), afterward the Arai slope returns to the expected trend until T_{ex} reaches the T_{ub} of the SMMs at 520°C when additional TRM is gained and the slope deviates from the expected slope again.

Changing the concentration of the SMMs at each step modifies the shape of the corresponding segments on the Arai plot. This is the same effect as for the static-accumulation model.

4. Linear Algebra Notation and Assessment of pTRM Checks

The preceding cases demonstrate that by controlling the concentration of SMMs, it is possible to produce a broad range of shapes on the Arai plot. The nonlinear types of behavior can readily be identified by visual inspection. Of more concern, however, are the cases that yield linear Arai plots. When combined with acceptable pTRM check statistics, such behavior is often viewed as necessary indicators of a reliable paleointensity estimate. It is therefore important to assess if this empirical conclusion is justified when neoformation occurs.

We note that our paleointensity models can be expressed as the solution to a general linear algebraic problem when the GSDs of SMMs at each temperature step are considered as known variables. Full details of the formulation of model in this form are given in the supporting information. By taking this approach, it can be demonstrated that linear Arai plots are possible even in the presence of the formation of new magnetic minerals, provided that the minimum T_b of the newly formed SMMs at each step is lower than its T_f. We term such a linear Arai plot behavior as a pseudoideal Arai plot because, although linear, the slope differs from the expected ideal value. Being able to consistently produce pseudoideal data, we can then quantitatively investigate how pTRM checks and the deviations of the paleointensity estimations are related in the context of neoformation.

4.1. Linear Algebra Notation of the Previous Models

The slope of the segment between two adjacent points on the Arai plot is $pNRM(T_i,T_{i+1})/pTRM(T_i,T_{i+1})$, where $pTRM(T_i,T_{i+1})$ is the pTRM gained between T_i and T_{i+1} (i.e., the difference between $pTRM(T_0,T_i)$ and $pTRM(T_0,T_{i+1})$). For the static-accumulation model, the difference between the pseudoideal and the ideal slope, which is -1 for $B_{anc} = B_{lab}$, of the segment within $[T_i,T_{i+1}]$ results from all SMMs that are produced up to T_{i+1} with T_b between T_i and T_{i+1}. That is,

$$\left|\frac{pTRM(T_i,T_j)}{pNRM(T_i,T_j)}\right| = 1 + \frac{\sum_{k=1}^{i} c_k p_{kij} + c_j p_{j0j}}{n_{ij}}, \tag{14}$$

where $j = i + 1$, $n_{ij} = pNRM(T_i,T_j)$, c_k is the concentration of SMMs formed at T_k and $c_k p_{kij}$ represents the contribution to $pTRM(T_i,T_j)$ from the SMMs formed at step k. With the assumption that T_b is only a function of volume, $p_{kij} = \int_{V_B(T_i)}^{V_B(T_j)} g_k(V) M_{tr}(T_0, V) V dV$ is used for demonstration, but not for derivation listed in the supporting information, therefore our expressions and the later discussion has a general sense.

We define

$$\alpha_{ij} = \frac{\sum_{k=1}^{i} c_k p_{kij} + c_j p_{j0j}}{n_{ij}} \tag{15}$$

as the deviation factor, which is the deviation of resultant 1/slope from the expected value of the segment within $[T_i,T_j]$. Physically, α_{ij} is the proportion of secondary $pTRM(T_i,T_j)$ to primary $pNRM(T_i,T_j)$. For a pseudoideal Arai plot, $\alpha_{ij} = \alpha$ for all temperature intervals, which means the increase of secondary pTRM at any step is α times of the primary pNRM over the same temperature interval. For an experiment with N heating steps, equation (15) can be written in a linear algebraic form:

$$\mathbf{Pc} = \mathbf{n}, \tag{16}$$

where $\mathbf{P}=\begin{bmatrix} p_{101} & & & & & & 0 \\ p_{112} & p_{202} & & & & & \\ \vdots & \vdots & \ddots & & & & \\ p_{1(k-1)k} & p_{2(k-1)k} & \cdots & p_{k0k} & & & \\ \vdots & \vdots & \ddots & \vdots & \ddots & & \\ p_{1(N-1)N} & p_{2(N-1)N} & \cdots & p_{k(N-1)N} & \cdots & p_{N0N} \end{bmatrix}$ with each column being proportional to the pTRM spectrum of SMMs formed at the corresponding step, $\mathbf{c} = (c_1, \ldots, c_k, \ldots, c_N)^{\mathrm{T}}$ and $\mathbf{n} = \alpha(n_{01}, \ldots, n_{(k-1)k}, \ldots, n_{(N-1)N})^{\mathrm{T}}$.

Given the value of α, $\mathbf{c}$ is unique if $\mathbf{P}$ is invertible. Since $\mathbf{P}$ is a lower triangular matrix, it is invertible if the diagonal elements are nonzero, which can be satisfied as long as the SMMs are partly unblocked when formed (i.e., $\min(T_b) < T_f$) so that $p_{k0k} > 0$. Given that our models assume neoformation of magnetic minerals, and not destruction, $c_k > 0$. Under these conditions, the unique solution for $\mathbf{c}$ that yields a linear Arai plot can be expressed as:

$$\mathbf{c}=\alpha\mathbf{P}^{-1}\mathbf{n} \equiv \alpha\mathbf{n}^{*}. \tag{17}$$

The general form of equation (16), which is valid for both linear and nonlinear Arai plots, is:

$$\mathbf{Pc}=\mathbf{N}\alpha, \tag{18}$$

where $\mathbf{N} = \mathrm{diag}(n_{01}, \ldots, n_{(k-1)k}, \ldots, n_{(N-1)N})$ and $\boldsymbol{\alpha} = (\alpha_1, \ldots, \alpha_k, \ldots, \alpha_N)^{\mathrm{T}}$. Rearrangement of (18) yields:

$$\boldsymbol{\alpha}=\mathbf{N}^{-1}\mathbf{Pc}. \tag{19}$$

Equation (19) encompasses the three parameters that can influence the slope of the Arai plot in the static-accumulation model: $\mathbf{N}^{-1}$ is related to the GSD of the PMM (hence the T_b distribution of the PMM), and $\mathbf{P}$ and $\mathbf{c}$ are related to the GSD and the concentration of the SMM, respectively.

Equations (16–19) remain valid for the dynamic model with:

$$\mathbf{P}_{\mathrm{dyn}} = \begin{bmatrix} p_{101} & & & & & & & 0 \\ -p_{101} & p_{202} & & & & & & \\ 0 & -p_{202} & p_{303} & & & & & \\ \vdots & \vdots & \vdots & \ddots & & & & \\ 0 & 0 & 0 & \cdots & p_{k0k} & & & \\ \vdots & \vdots & \vdots & \ddots & \vdots & \ddots & & \\ 0 & 0 & 0 & \cdots & 0 & \cdots & p_{(N-1)0(N-1)} & \\ 0 & 0 & 0 & \cdots & 0 & \cdots & -p_{(N-1)0(N-1)} & p_{N0N} \end{bmatrix}.$$

The dynamic-growth model, however, dictates that the total volume of newly formed magnetic phase must not decrease. Therefore, a solution for $\mathbf{c}$ will be accepted only if it satisfies this constraint.

Two cases of pseudoideal Arai plots are illustrated in Figure 6. The elements in $\mathbf{P}$ and $\mathbf{P}_{\mathrm{dyn}}$ are calculated for these special cases. D_{median}'s and σ's for secondary GSDs are the same for both cases, c's are obtained by solving equation (15) to find solutions that satisfy the assumptions. Both cases result in identical paleointensity estimates and the variation of M_{rs} are almost the same below 450°C (Figure 6c). The pTRM check behavior, which will be discussed in the next section, is different.

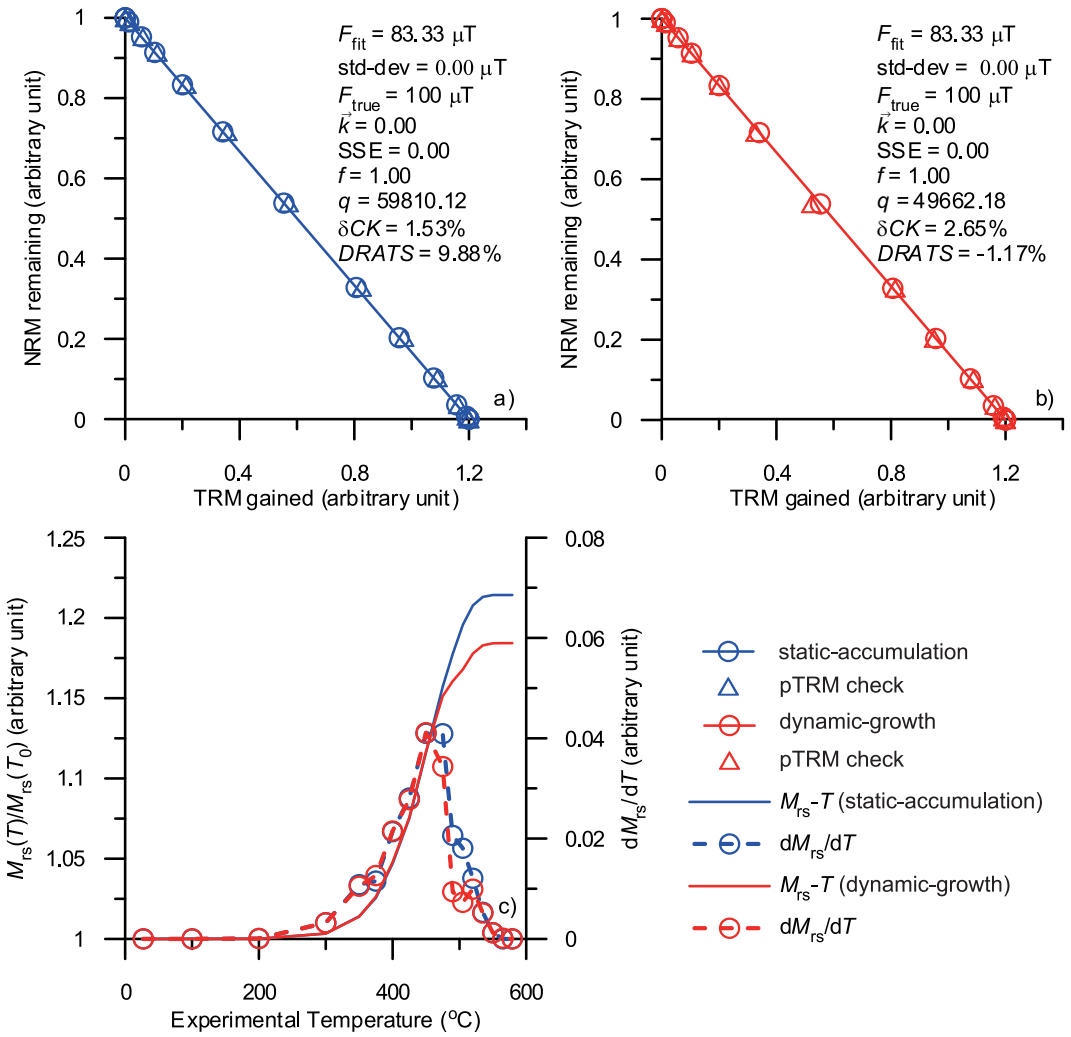

Figure 6. Pseudoideal Arai plots (slope = −1/1.2) from (a) the static-accumulation model and (b) the dynamic-growth model. The slopes are the same, deviating from the expected value of −1. For the static-accumulation model, pTRM checks are systematically larger than the original pTRMs. For the dynamic-growth model, pTRM checks can be smaller than the original pTRMs. Circles are the original pTRMs and triangles are the pTRM checks. Their corresponding M_{rs}-T_{ex} curves and the first derivatives are shown in Figure 6c.

4.2. pTRM Check Criteria and Their Dependence on Magnetic Granulometry

pTRM checks are a routine procedure in Thellier-type paleointensity experiments and aim to diagnose any alteration that affects the behavior of pTRM acquisition in a specimen. Thus, far we have described pTRM checks in a qualitative fashion, but numerous methods exist for the quantification of pTRM checks. There is still debate as to which method is the most appropriate for quantifying pTRM checks and which critical values should be used to select data and numerous studies have suggested new statistics or new selection thresholds [e.g., *Selkin and Tauxe*, 2000; *Kissel and Laj*, 2004; *Paterson et al*., 2012]. For the sake of brevity and illustrative purposes, we will investigate two pTRM statistics using our two models of pseudoideal data. First, we consider δCK, which is the maximum absolute pTRM check difference normalized by the intercept of the best fit line on the x axis of the Arai plot ($X_{Int.}$):

$$\delta CK = \frac{\max\left\{\left|\delta pTRM_{i,j}\right|\right\}}{X_{Int.}} \times 100. \tag{20}$$

Second, we consider the cumulative pTRM check statistic, *DRATS*, which is given by:

$$DRATS = \frac{\sum_{i=start}^{end} \delta pTRM_{i,j}}{pTRM(T_0, T_{end})} \times 100, \tag{21}$$

where "*start*" and "*end*" denote the first and last temperature step used for the best fit analysis, respectively, and $pTRM(T_0, T_{end})$ represents the pTRM gained at this last step. Typically, *DRATS* is taken to be the sum of the absolute values of pTRM check differences, however, we use the sum of signed values (i.e., $\pm\delta pTRM_{i,j}$) to investigate the manifestation of alteration in our models. When $DRATS < 0$, the pTRM checks tend to be less than the original TRMs, and vice versa. When applied to selecting real data, it is common to require that $\delta CK \leq 5$–10% and/or $DRATS \leq 10$–20%. These threshold values are chosen empirically based on analysis on extensive data [*Kissel and Laj*, 2004] or data set specific analyses [*Ben-Yosef et al*., 2008; *Shaar and Tauxe*, 2013]. Although recent work is refining how this choice is made [e.g., *Paterson et al*., 2012, 2014], the specific relation between the pTRM check statistics and the accuracy of a paleointensity estimate in the presence of alteration remains unclear.

For our pseudoideal Arai plots, since we can use the entire Arai plot segment for analysis, $pTRM(T_0,T_{end})$ is $X_{Int.}$ by definition and thus *DRATS* can be viewed as the cumulative equivalent of δCK. In the terminology of our model the normalizer of these two statistics can be expressed as $(1 + \alpha)p$, which assumes that the PMMs have a total TRM of p when $B_{lab} = B_{anc}$ and the SMMs have increased the TRM α times. In the static-accumulation model,

$$pTRM(T_0, T_i) = p_{00i} + \sum_{k=1}^{i} c_k p_{k0i}, \tag{22}$$

and

$$pTRM'_j(T_0, T_i) = p_{00i} + \sum_{k=1}^{j} c_k p_{k0i} \quad (j = i+1), \tag{23}$$

where p_{00i} is the TRM acquired by the PMMs. By substituting equations (22), (23) and $c_i = \alpha n_i^*$ (equation (17)) into (9), we have

$$\delta pTRM_{i,j} = c_j p_{j0i} = \alpha n_j^* p_{j0i}.$$

δCK can be expressed as:

$$\delta CK = \frac{1}{\left(1+\frac{1}{\alpha}\right)} \frac{\max\left\{n_j^* p_{j0i}\right\}}{p} \times 100 \equiv u_\alpha \frac{\max\left\{n_j^* p_{j0i}\right\}}{p} \times 100, \tag{24}$$

and *DRATS* as:

$$DRATS = \frac{u_\alpha}{p} \sum_{i=start}^{end-\Delta i} n_j^* p_{j0i} \times 100, \tag{25}$$

where Δi is the step increment between the original pTRM and the check step.

It can be noted that the factor u_α is the relative underestimate of the true paleointensity, which is $(B_T - B_E)/B_T$ with B_T and B_E being the true and estimated paleointensity.

For the dynamic-growth model,

$$\delta CK = \frac{u_\alpha}{p} \max\left\{\left|n_j^* p_{j0i} - n_i^* p_{i0i}\right|\right\} \times 100, \tag{26}$$

and

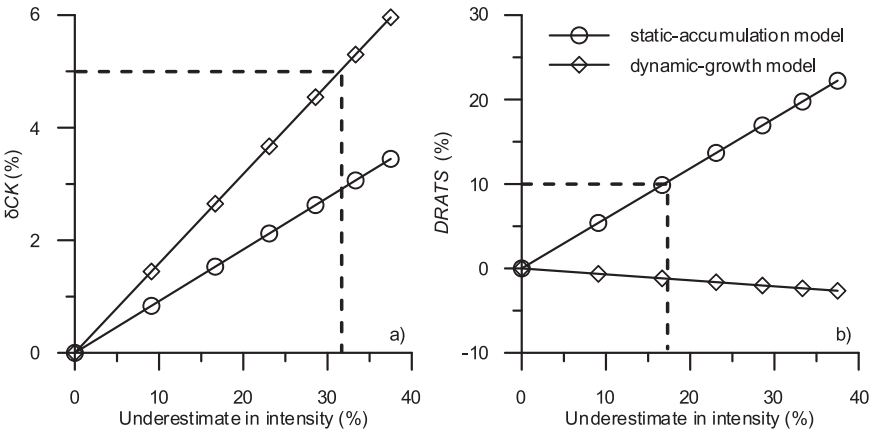

Figure 7. δCK and *DRATS* as functions of the paleointensity underestimate with respect to the expected intensity. For both the static-accumulation model and the dynamic-growth model, parameters for coercivity and GSDs of PMMs and SMMs are the same. $\delta CK \leq 5\%$ and $DRATS \leq 10\%$ are typical thresholds used to screen to data.

$$DRATS = \frac{u_\alpha}{p}\left(n^*_{end}p_{end0end} - \sum_{i=start+\Delta i}^{end-\Delta i} n^*_i p_{i(i-\Delta i)i} - n^*_{start}p_{start0start}\right)\times 100. \quad (27)$$

For the simulation shown in Figure 6, $start = 1$, $end = 16$, and $\Delta i = 1$.

From equations (24) to (27) it is clear that δCK and *DRATS* are positively correlated to u_α. That is to say, both the static-accumulation and the dynamic-growth models predict that the two statistics are functions of the degree of misestimation from these pseudoideal Arai plots. The equations, however, also indicate that the statistics are influenced by the distribution of both the PMM and the SMM, as given by the term $n^*_k p_{k0i}$. Therefore, results with the same δCK or *DRATS* may have different degrees of deviation from the true value. It is also possible for two specimens to experience different alteration processes, that yield the same u_α (i.e., the same deviation of the paleointensity estimate from the expected value), but have largely different δCK and *DRATS* values. This is illustrated in Figure 7. The GSDs of PMMs and SMMs are the same as the cases shown in Figure 6 where solutions to equation (16) exist for a wide range of u_α. The δCK and *DRATS* of corresponding pseudoideal Arai plots are numerically calculated with increasing u_α. If an absolute value of $\delta CK \leq 5\%$ were used to screen data (Figure 7a), the static-accumulation cases would pass the check with significant underestimates and the dynamic-growth cases would pass the check with underestimates of up to ~30%. If $DRATS \leq 10\%$ were used (Figure 7b), underestimates for the static-accumulation cases would be reduced to ~17%. For the dynamic-growth cases, *DRATS* is not as sensitive as δCK and all DRATS are <10%, despite underestimates of up to ~37%.

5. Discussion

5.1. Arai Plot Behavior Due to Alteration

Equation (19) predicts that ideal specimens that experience the growth of new magnetic phases can yield a range of Arai plot behavior, which depends on the magnetic granulometry and concentration of both PMMs and SMMs.

Pseudoideal Arai plots that result from alteration have been documented in the literature. *Kono* [1987] found that TRM can be linearly proportional to NRM even though secondary magnetic phases formed through oxidation during laboratory heating. Similarly, studies *Prévot et al.* [1983, 1985] observed that Arai plots with large linear sections can result from thermally altered specimens, which lead to underestimate. More recently, *Cottrell and Tarduno* [2000] obtained paleointensity estimates from linear sections on Arai plots of whole rock samples, which are lower than the results from single plagioclase crystals. They argued that this lower estimate was the result of neoformation in whole rocks.

Concave-up Arai plots are most commonly associated with multidomain (MD) behavior [e.g., *Levi*, 1977] or multiple components of magnetization [e.g., *Yu and Dunlop*, 2002]. Although they have also been

suggested to result from alteration, this work provides the first unambiguous evidence that this is a viable mechanism.

Concave-down Arai plots are much less common, but have been reported for multiple components of magnetization [e.g., *Yu and Dunlop*, 2002] and MD effects [*Shaar et al*., 2011], but have also been suggested to result from alteration [e.g., *Paterson*, 2011]. The lack of wide spread reporting in the literature may be due to the potential disguising of such behavior. Consider a case where the PMMs and SMMs are MD and SD particles, respectively. If the static-accumulating SMMs result in concave-down shape with $\delta pTRM_{i,j} > 0$, it probably will be disguised by the primary MD components which is concave-up with $\delta pTRM_{i,j} < 0$. Therefore, the resultant plot is less curved and may pass remanence checks and may resemble an ideal SD behavior without further verification.

Tauxe and Love [2003] postulated the appearance of two shifted, but parallel linear sections on Arai plot, which may arise from alteration with a discrete T_b that is higher than its T_f. We predict this behavior in our models, and if the SMMs have $T_b < T_f$, the shift could also be abrupt even with a finite distribution (Figure 3). The narrow T_b distribution of the SMMs spans an interval of 50°C (Figure 3a, blue) and the shift takes place within a interval of 25°C when $T_b < T_f$ (Figure 3d, 450–475°C), whereas the shift takes place within a interval of 50°C if $T_b > T_f$ (Figure 3c, 400–450°C). The other shape is characterized by a "Z" pattern where the pTRM at a higher temperature is smaller than the preceding pTRM as is seen at around 425°C in Figure 5d. *Herrero-Bervera and Valet* [2009] reported a similar pattern that was often observed below 300°C in their study (see their Figures 7a–7c). Though they perform the first heating-cooling in field, the Arai plot is likely similar to that obtained by the Coe experiment if TCRM was absence. Therefore, the behavior that they see in their results might be a consequence of the fast growth of SMMs, which probably have a high T_b component, and may be due to oxidation of low T_b components [*Kono*, 1987].

5.2. Mechanism of pTRM Checks for SD Particles

A pTRM check at T_i is only sensitive to a fraction of the new magnetic particles that form between the original step (T_i) and the check step after heating to T_j ($T_i < T_f < T_j$). Components of neoformation with $T_b > T_i$ are invisible. In other words, pTRM checks are only able to capture neoformation with (1) $T_i < T_f < T_j$ and (2) $T_b < T_i$. As an extreme example of the static-accumulation model (Figures 3c and 3e), if new minerals formed in zero-field between two steps are all in a blocked state at T_i (i.e., $T_b > T_f > T_i$), the pTRM check is totally ineffective. Moreover, these components cannot be detected by subsequent pTRM checks at elevated temperature windows ($[T_{i+}, T_{j+}]$) either, since $T_f < T_{i+}$. Nevertheless, the corresponding Arai plot slope can be distorted significantly. For the dynamic-growth model on the other hand, T_f is not constant since the SMMs can evolve with temperature. Therefore, the SMMs initially formed at T_i are likely to influence several pTRM check steps depending on their growth rate (i.e., the increase of T_b).

Valet et al. [1996] proposed a method to correct pTRMs based on pTRM checks under the assumption that the pTRM check differences were due to alteration [see also *McClelland and Briden*, 1996]. The underlying assumptions of the method are that (1) the SMMs produced at one step (T_i) are fully unblocked at T_{i-1} (i.e., $T_{b\_sec} < T_{i-1} < T_f = T_i$) and that (2) existing SMMs remain the same in subsequent steps since $pTRM(T_0,T_i)$ was explicitly assumed not to change. The second assumption in fact coincides with the static-accumulation model. When the assumptions are satisfied, the pTRM check difference at T_{i-1} (denoted as $\delta pTRM_{i-1,i}$) will measure all the creation of magnetic phase between T_{i-1} and T_i and the $\delta pTRM_{i-1,i}$ values are additive (i.e., they are carried by SD particles under assumption 2). Therefore, the measured $pTRM(T_0,T_i)$ is the sum of the ideal $pTRM(T_0,T_i)$ and the cumulative sum of all $\delta pTRM_{i-1,i}$ up to the T_i step. The "true" $pTRM(T_0,T_i)$ can then be recovered by subtraction. Verifying these two assumptions in practice is, however, extremely difficult; even in our static-accumulation model, there is no strict requirement that $T_{b\_sec} < T_{i-1} < T_f$. Therefore, the application of this type of correction is considered problematic [*Tauxe and Yamzaki*, 2007]. We demonstrate two examples of applying the correction of *Valet et al*. [1996] to the static-accumulation model (Figure 8). $pTRM(T_i,T_j)$ of the SMMs is set to be 20% of the primary pNRM over the same temperature interval ($\alpha = 0.2$) for both cases. In Figure 8a, the SMMs are formed in unblocked states. Since the SMMs affect pTRM effectively, *DRATS* exceeds common selection thresholds despite the linear shape of Arai plot and the acceptable value of δCK. After correction, however, the estimate is within 0.22 μT of the expected value. For the example in Figure 8b, the SMMs are formed in a partially unblocked state. The resulting Arai plot is also linear with acceptable δCK and *DRATS*. The uncorrected data yield an

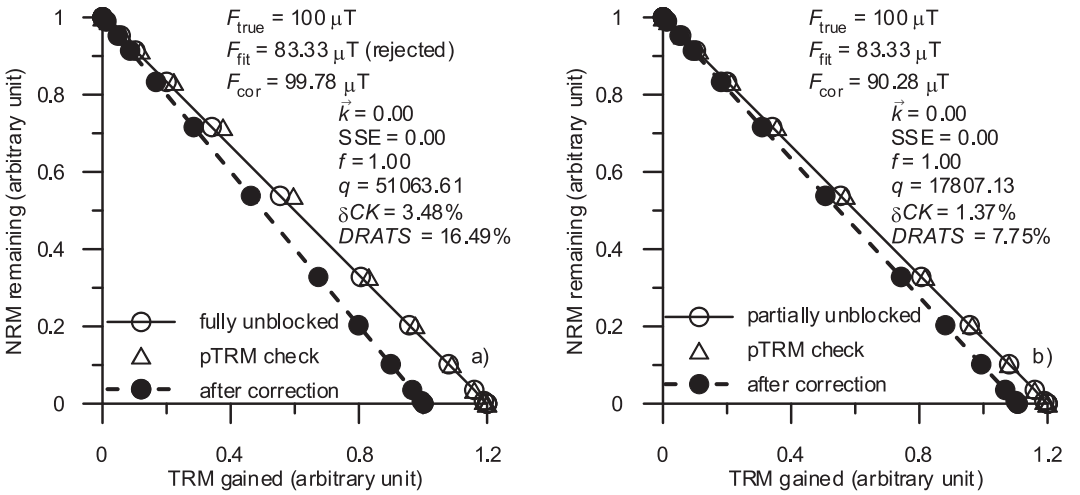

Figure 8. Examples of the pTRM correction of *Valet et al*. [1996] applied to the static-accumulation model. Data after correction (dashed line with solid dots) are compared with raw data. (a) SMMs are formed in an unblocked state, which satisfies the first assumption of this correction method. *DRATS* would fail to pass typical selection thresholds, therefore the F_{fit} is rejected. However, the corrected estimate is almost equal to the true field. (b) SMMs are formed in a partially unblocked state, which violates the assumptions of the correction. The corrected estimate is still ∼10% lower than the true field.

underestimate that is ∼16% lower than the expected value. The correction reduces this underestimate to ∼10% (an estimate of 90.25 μT). This result is acceptable given that a paleointensity estimate has been suggested to have a precision no better than ∼20% [*Valet*, 2003]. However, it should be noted from the two cases, that a better estimate could be derived from seemingly bad data, as suggested by remanence checks.

5.3. Other Alteration Mechanisms

CRM and TCRM are important secondary remanences that jeopardize the fidelity of paleointensity determinations. These mechanisms also present the possibility of obtaining a high-quality linear Arai plot if the NRM of a specimen is of TCRM origin rather than TRM [e.g., *McClelland*, 1996; *Fabian*, 2009]. They may also occur in the laboratory during in-field thermal treatments. If SMMs continue growing in-field during cooling whereby their T_b's exceed the corresponding T_{ex}, the acquired TCRM would be superimposed on the NRM remaining. In this case, if the laboratory field direction is not parallel to the NRM direction, although pseudoideal Arai plots may still be possible, NRM vectors on the Zijderveld plot [*Zijderveld*, 1967] will progressively deviate toward the laboratory field direction. Directional statistics such as the maximum angular deviation [*Kirschvink*, 1980] and the deviation angle [*Tauxe and Staudigel*, 2004] might then be useful to identify the alteration if it is significant. Therefore, assuming that neoformation is prone to take place in the first heating-cooling at each T_{ex}, other Thellier-type experiments [i.e., the original Thellier-Thellier, the Aitken, and IZZI protocols] may be more likely to reveal alteration than the Coe protocol. In addition, in the presence of CRM and/or TCRM acquisition pTRM tail checks [*McClelland and Briden*, 1996; *Riisager and Riisager*, 2001] may prove to be a useful tool to detect alteration.

This study illustrates that the neoformation of magnetic minerals could be responsible for paleointensity underestimates. Paleointensity overestimates, on the other hand, are commonly reported in studies that use Thellier-type experiments. Although reasons such as the influence of cooling rate [e.g., *Fox and Aitken*, 1980] or the effects of CRM and TCRM [e.g., *McClelland*, 1996; *Yamamoto et al*., 2003; *Fabian*, 2009] can explain some overestimates, alteration effects such as oxidation during laboratory heating procedures may also be responsible. Progressive oxidation of the PMMs (e.g., magnetite) to less magnetic minerals (e.g., maghemite and hematite) may not be directly detected by pTRM checks and would depend on the oxidation rate with respect to the unblocking of NRM. In such cases, the NRM loss during demagnetization is due to two factors: the inherent thermal demagnetization of NRM and the decrease of the intrinsic M_s. Decreases in M_s will also lower the subsequent pTRMs. The overall effects could be that the ratio of |NRM/TRM| increases and results in an overestimate of the paleointensity, possibly with acceptable pTRM check statistics.

We have demonstrated that the passing of pTRM check based data selection may not be sufficient to successfully screen paleointensity data. When only neoformation or oxidation happens, M_{rs} may be more sensitive to the alteration. However, when several types of alteration happen simultaneously, changes in M_{rs} may cancel each other out and other monitoring methods are necessary. The anhysteretic remanent magnetization (ARM) and FORC diagrams [*Pike et al*., 1999] provide detailed information on coercivity distributions and therefore could be capable of revealing insightful information on laboratory alteration [e.g., *Carvallo et al*., 2006; *de Groot et al*., 2012]. It should be noted that these high field measurements have to be performed on sister specimens, which may significantly different from each other and may not be representative of the paleointensity specimen [*Tauxe and Staudigel*, 2004]. Although low-field susceptibility measurements can be performed on the same specimen before and after paleointensity experiments, a number of studies indicate that monitoring changes in room temperature magnetic susceptibility may not be suitable for unambiguously identifying magnetic alteration [e.g., *Biggin and Thomas*, 2003; *Pressling et al*., 2006; *Paterson et al*., 2010] because susceptibility is affected also by materials other than remanence carriers.

6. Conclusions

The Coe paleointensity protocol, although commonly used in paleointensity determinations, is subject to mineralogical alteration due to the intensive heating procedure required. Investigation of the effects of the formation of secondary magnetic minerals (in the absence of CRM/TCRM acquisition) has been simulated for a Coe paleointensity protocol conducted on specimens containing SD magnetite. Our numerical simulations suggest that neoformation can produce a variety of Arai plot behavior (e.g., linear, concave-up, and concave-down), which is controlled by the concentration and the distribution of blocking temperatures (T_b) of both the primary and secondary phases. In particular, when secondary magnetic phases occur with relatively wide T_b distributions combined with appropriate concentrations, pseudoideal Arai plots are possible, which confirms previous experimental suggestions [e.g., *Prévot et al*., 1983, 1985]. Such Arai plots can unfortunately lead to large underestimates of the true paleointensity.

Concerning neoformation, secondary magnetic minerals that form at low temperatures, but have high T_b, cannot be detected by pTRM checks. In general, pTRM checks depend on the magnetic properties of both primary and secondary magnetic phases in a complex fashion and the sliding pTRM check will effectively identify the alteration only if the majority of the T_b spectra of the secondary phases are lower than their formation temperature. As a consequence certain alteration mechanisms may not be detected by commonly used pTRM check statistics (e.g., δCK or *DRATS*) and pTRM checks, while necessary, may not be sufficient to monitor alteration during Coe protocol experiments. Other magnetic measurements are highly recommended to complement the paleointensity data in order to exclude any under/overestimate that is not detectable by routine pTRM checks.

Appendix A: Summary of the Acronyms and Notations of Major Terms Used in This Paper

B_0	the external magnetic field in Tesla.
B_k	the microscopic coercivity of magnetic minerals.
c	concentration (number of particles relative to number of primary particles).
D_{median}	median diameter of magnetic particles.
$g(V;\mu,\sigma)$ or $g(V)$	grain size distribution (GSD).
$g_{pri}(V)$	GSD of the PMM.
$g^*(V,T_i)$	The effective GSD of all magnetic particles up to the ith step.
$M_{tr}(T_0,V)$	magnetization of TRM of magnetite with volume V cooling from T_b to T_0.
n_{ij}	partial NRM of the PMMs acquired between T_i and T_j.
p	total TRM of the PMM.
p_{kij}	$pTRM(T_i,T_j)$ of SMMs formed at $T = T_k$ with $c = 1$.
PMM	primary magnetic mineral.
$pNRM(T_i,T_j)$	partial NRM acquired between T_i and T_j.
$pTRM(T_i,T_j)$	partial TRM acquired between T_i and T_j.

SMM	secondary magnetic mineral.
T_0	room temperature.
T_b	blocking temperature.
T_f	formation temperature of SMMs.
T_i	experimental temperature for step *i*.
T_{ub}	unblocking temperature.
α_{ij}	deviation of 1/slope from the expected value between T_i and T_j.
μ	the location parameter of the log-normal distribution.
σ	the shape parameter of the log-normal distribution.

Acknowledgments

The manuscript was significantly improved through the reviews of Lisa Tauxe and Mark Dekkers. We acknowledge their constructive suggestions. We would like to thank James Tyburczy and David Heslop for their work during the review. This work was supported by the National Natural Science Foundation of China (grants 41374073, 41025013, and 40821091), the German Research Foundation (DFG grants EG294/2-1), and the National Research Foundation of Korea (NRF) grant funded by the Korea government (MSIP) (NRF-2013R1A2A1A01004418). Greig A. Paterson acknowledges funding from the Key Laboratory of Earth's Deep Interior, IGGCAS.

References

Aitken, M. J., A. L. Allsop, G. D. Bussell, and M. B. Winter (1988), Determination of the intensity of the Earth's magnetic field during archaeological times: Reliability of the Thellier technique, *Rev. Geophys.*, *26*, 3–12, doi:10.1029/RG026i001p00003.

Ben-Yosef, E., H. Ron, L. Tauxe, A. Agnon, A. Genevey, T. E. Levy, U. Avner, and M. Najjar (2008), Application of copper slag in geomagnetic archaeointensity research, *J. Geophys. Res.*, *113*, B08101, doi:10.1029/2007JB005235.

Biggin, A. J., and D. N. Thomas (2003), The application of acceptance criteria to results of Thellier palaeointensity experiments performed on samples with pseudosingle-domain-like characteristics, *Phys. Earth Planet. Inter.*, *138*, 279–287, doi:10.1016/S0031-9201(03)00127-4.

Carvallo, C., A. P. Roberts, R. Leonhardt, C. Laj, C. Kissel, M. Perrin, and P. Camps (2006), Increasing the efficiency of paleointensity analyses by selection of samples using first-order reversal curve diagrams, *J. Geophys. Res.*, *111*, B12103, doi:10.1029/2005JB004126.

Coe, R. S. (1967), Paleo-intensities of the Earth's magnetic field determined from tertiary and quaternary rocks, *J. Geophys. Res.*, *72*, 3247–3262, doi:10.1029/JZ072i012p03247.

Cottrell, R. D., and J. A. Tarduno (2000), In search of high-fidelity geomagnetic paleointensities: A comparison of single plagioclase crystal and whole rock Thellier-Thellier analyses, *J. Geophys. Res.*, *105*, 23,579–23,594, doi:10.1029/2000JB900219.

de Groot, L. V., M. J. Dekkers, and T. A. Mullender (2012), Exploring the potential of acquisition curves of the anhysteretic remanent magnetization as a tool to detect subtle magnetic alteration induced by heating, *Phys. Earth Planet. Inter.*, *194*, 71–84, doi:10.1016/j.pepi.2012.01.006.

Draeger, U., M. Prévot, T. Poidras, and J. Riisager (2006), Single-domain chemical, thermochemical and thermal remanences in a basaltic rock, *Geophys. J. Int.*, *166*, 12–32. doi:10.1111/j.1365-246X.2006.02862.x.

Dunlop, D. J., and Ö. Özdemir (1997), *Rock Magnetism: Fundamentals and Frontiers, Cambridge Studies in Magnetism*, Cambridge Univ. Press, New York.

Fabian, K. (2009), Thermochemical remanence acquisition in single-domain particle ensembles: A case for possible overestimation of the geomagnetic paleointensity, *Geochem. Geophys. Geosyst.*, *10*, Q06Z03, doi:10.1029/2009GC002420.

Fox, J. M. W., and M. J. Aitken (1980), Cooling-rate dependence of thermoremanent magnetisation, *Nature*, *283*, 462–463, doi:10.1038/283462a0.

Herrero-Bervera, E., and J. P. Valet (2009), Testing determinations of absolute paleointensity from the 1955 and 1960 Hawaiian flows, *Earth Planet. Sci. Lett.*, *287*, 420–433, doi:10.1016/j.epsl.2009.08.035.

Kissel, C., and C. Laj (2004), Improvements in procedure and paleointensity selection criteria (PICRIT-03) for Thellier and Thellier determinations: Application to Hawaiian basaltic long cores, *Phys. Earth Planet. Inter.*, *147*, 155–169, doi:10.1016/j.pepi.2004.06.010.

Kirschvink, J. L. (1980), The least-squares line and plane and the analysis of palaeomagnetic data, *Geophys. J. R. Astron. Soc.*, *62*, 699–718, doi:10.1111/j.1365-246X.1980.tb02601.x.

Koenigsberger, J. (1936), Die abhaengigkeit der natuerlichen remanenten magnetisierung bei eruptivgesteinen von deren alter und zusammensetzung, *Beitr. Angew. Geophys.*, *5*, 193–246.

Kono, M. (1987), Changes in TRM and ARM in a basalt due to laboratory heating, *Phys. Earth Planet. Inter.*, *46*, 1–8, doi:10.1016/0031-9201(87)90167-1.

Kosterov, A. A., and M. Prévot (1998), Possible mechanisms causing failure of Thellier palaeointensity experiments in some basalts, *Geophys. J. Int.*, *134*, 554–572, doi:10.1046/j.1365-246x.1998.00581.x.

Levi, S. (1977), The effect of magnetite particle size on paleointensity determinations of the geomagnetic field, *Phys. Earth Planet. Inter.*, *13*, 245–259, doi:10.1016/0031-9201(77)90107-8.

McClelland, E. (1996), Theory of CRM acquired by grain growth, and its implications for TRM discrimination and palaeointensity determination in igneous rocks, *Geophys. J. Int.*, *126*, 271–280, doi:10.1111/j.1365-246X.1996.tb05285.x.

McClelland, E., and J. C. Briden (1996), An improved methodology for Thellier-type paleointensity determination in igneous rocks and its usefulness for verifying primary thermoremanence, *J. Geophys. Res.*, *101*, 21,995–22,013, doi:10.1029/96JB02113.

Nagata, T., Y. Arai, and K. Momose (1963), Secular variation of the geomagnetic total force during the last 5,000 years, *J. Geophys. Res.*, *68*, 5277–5281.

Néel, L. (1949), Théorie du traînage magnétique des ferromagnétiques en grains fins avec applications aux terres cuites, *Ann. Géophys.*, *5*, 99–136.

Paterson, G. A. (2011), A simple test for the presence of multidomain behaviour during paleointensity experiments, *J. Geophys. Res.*, *116*, B10104, doi:10.1029/2011JB008369.

Paterson, G. A. (2013), The effects of anisotropic and non-linear thermoremanent magnetizations on Thellier-type paleointensity data, *Geophys. J. Int.*, *193*, 694–710, doi:10.1093/gji/ggt033.

Paterson, G. A., A. R. Muxworthy, A. P. Roberts, and C. Mac Niocaill (2010), Assessment of the usefulness of lithic clasts from pyroclastic deposits for paleointensity determination, *J. Geophys. Res.*, *115*, B03104, doi:10.1029/2009JB006475.

Paterson, G. A., A. J. Biggin, Y. Yamamoto, and Y. Pan (2012), Towards the robust selection of Thellier-type paleointensity data: The influence of experimental noise, *Geochem. Geophys. Geosyst.*, *13*, Q05Z43, doi:10.1029/2012GC004046.

Paterson, G. A., L. Tauxe, A. J. Biggin, R. Shaar, and L. C. Jonestrask (2014), On improving the selection of Thellier-type paleointensity data, *Geochem. Geophys. Geosyst.*, doi:10.1002/2013GC005135, in press.

Pike, C. R., A. P. Roberts, and K. L. Verosub (1999), Characterizing interactions in fine magnetic particle systems using first order reversal curves, *J. Appl. Phys.*, *85*, 6660–6667, doi:10.1063/1.370176.

Pressling, N., C. Laj, C. Kissel, D. Champion, and D. Gubbins (2006), Palaeomagnetic intensities from ^{14}C-dated lava flows on the Big Island, Hawaii: 0–21 kyr, *Earth Planet. Sci. Lett.*, *247*, 26–40, doi:10.1016/j.epsl.2006.04.026.

Prévot, M., E. A. Mankinen, S. Grommé, and A. Lecaille (1983), High paleointensities of the geomagnetic field from thermomagnetic studies on Rift Valley pillow basalts from the Mid-Atlantic Ridge, *J. Geophys. Res.*, *88*, 2316–2326, doi:10.1029/JB088iB03p02316.

Prévot, M., E. A. Mankinen, R. S. Coe, and C. S. Grommé (1985), The Steens Mountain (Oregon) geomagnetic polarity transition. 2: Field intensity variations and discussion of reversal models, *J. Geophys. Res.*, *90*, 10,417–10,448, doi:10.1029/JB090iB12p10417.

Qin, H., H. He, Q. Liu, and S. Cai (2011), Palaeointensity just at the onset of the Cretaceous normal superchron, *Phys. Earth Planet. Inter.*, *187*, 199–211, doi:10.1016/j.pepi.2011.05.009.

Riisager, P., and J. Riisager (2001), Detecting multidomain magnetic grains in Thellier palaeointensity experiments, *Phys. Earth Planet. Inter.*, *125*, 111–117, doi:10.1016/S0031-9201(01)00236-9.

Selkin, P. A., and L. Tauxe (2000), Long-term variations in palaeointensity, *Philos. Trans. R. Soc. London A*, *358*, 1065–1088, doi:10.1098/rsta.2000.0574.

Shaar, R., and L. Tauxe (2013), Thellier GUI: An integrated tool for analyzing paleointensity data from Thellier-type experiments, *Geochem. Geophys. Geosyst.*, *14*, 677–692, doi:10.1002/ggge.20062.

Shaar, R., H. Ron, L. Tauxe, R. Kessel, and A. Agnon (2011), Paleomagnetic field intensity derived from non-SD: Testing the Thellier IZZI technique on MD slag and a new bootstrap procedure, *Earth Planet. Sci. Lett.*, *310*, 213–224, doi:10.1016/j.epsl.2011.08.024.

Smirnov, A. V., J. A. Tarduno, and B. N. Pisakin (2003), Paleointensity of the early geodynamo (2.45 Ga) as recorded in Karelia: A single-crystal approach, *Geology*, *31*, 415–418, doi:10.1130/0091-7613(2003)031<0415:POTEGG>2.0.CO;2.

Tarduno, J. A., R. D. Cottrell, M. K. Watkeys, A. Hofmann, P. V. Doubrovine, E. E. Mamajek, D. Liu, D. G. Silbeck, L. P. Neukirch, and Y. Usui (2010), Geodynamo, solar wind, and magnetopause 3.4 to 3.45 billion years ago, *Science*, *327*(5970), 1238–1240, doi:10.1126/science.1183445.

Tauxe, L., and J. J. Love (2003), Paleointensity in Hawaiian Scientific Drilling Project Hole (HSDP2): Results from submarine basaltic glass, *Geochem. Geophys. Geosyst.*, *4*(2), 8702, doi:10.1029/2001GC000276.

Tauxe, L., and H. Staudigel (2004), Strength of the geomagnetic field in the Cretaceous Normal Superchron: New data from submarine basaltic glass of the Troodos Ophiolite, *Geochem. Geophys. Geosyst.*, *5*, Q02H06, doi:10.1029/2003GC000635.

Tauxe, L., and T. Yamazaki (2007), Paleointensities, in *Treatise on Geophysics*, vol. 5, *Geomagnetism*, edited by M. Kono, pp. 509–563, Elsevier, Amsterdam.

Thellier, E., and O. Thellier (1959), Sur l'intensité du champ magnétique terrestre dans le passé historique et géologique, *Ann. Géophys.*, *15*, 285–376.

Valet, J.-P. (2003), Time variations in geomagnetic intensity, *Rev. Geophys.*, *41*(1), 1004, doi:10.1029/2001RG000104, 1.

Valet, J.-P., J. Brassart, I. Le Meur, V. Soler, X. Quidelleur, E. Tric, and P.-Y. Gillot (1996), Absolute paleointensity and magnetomineralogical changes, *J. Geophys. Res.*, *101*, 25,029–25,044, doi:10.1029/96JB02115.

Wehland, F., R. Leonhardt, F. Vadeboin, and E. Appel (2005), Magnetic interaction analysis of basaltic samples and pre-selection for absolute palaeointensity measurements, *Geophys. J. Int.*, *162*, 315–320, doi:10.1111/j.1365-246X.2005.02429.x.

Worm, H.-U. (1998), On the superparamagnetic-stable single domain transition for magnetite, and frequency dependence of susceptibility, *Geophys. J. Int.*, *133*, 201–206, doi:10.1046/j.1365-246X.1998.1331468.x.

Yamamoto, Y., H. Tsunakawa, and H. Shibuya (2003), Palaeointensity study of the Hawaiian 1960 lava: implications for possible causes of erroneously high intensities, *Geophys. J. Int.*, *153*, 263–276, doi:10.1046/j.1365-246X.2003.01909.x.

Yu, Y., and D. J. Dunlop (2002), Multivectorial paleointensity determination from the Cordova Gabbro, southern Ontario, *Earth Planet. Sci. Lett.*, *203*, 983–998, doi:10.1016/S0012-821X(02)00900-7.

Yu, Y. J., L. Tauxe, and A. Genevey (2004), Toward an optimal geomagnetic field intensity determination technique, *Geochem. Geophys. Geosyst.*, *5*, Q02H07, doi:10.1029/2003GC000630.

Zijderveld, J. D. A. (1967), A.C. demagnetization of rocks: Analysis of results, in *Methods in Palaeomagnetism*, edited by D. W. Collinson, K. M. Creer, and S. K. Runcorn, pp. 256–286, Elsevier, New York.

Zhang, C., G. A. Paterson, and Q. Liu (2012), A new mechanism for the magnetic enhancement of hematite during heating: The role of clay minerals, *Stud. Geophys. Geod.*, *56*, 845–860, doi:10.1007/s11200-011-9018-4.

Zhou, W., D. R. Peacor, J. C. Alt, R. Van der Voo, and L. S. Kao (2001), TEM study of the alteration of interstitial glass in MORB by inorganic processes, *Chem. Geol.*, *174*, 365–376, doi:10.1016/S0009-2541(00)00295-3.